Inorganic Chemistry

Article

pubs.acs.org/IC

Computational Insights on the Geometrical Arrangements of Cu(II) with a Mixed-Donor N_3S_3 Macrobicyclic Ligand

Andrés G. Algarra,*[†,‡] Gabriel Aullón,[§] Paul V. Bernhardt,[∥] and Manuel Martínez[§]

[†]Departamento de Ciencia de los Materiales e Ingeniería Metalúrgica y Química Inorgánica, Facultad de Ciencias, Universidad de Cádiz, Apartado 40, Puerto Real, 11510 Cádiz, Spain

[§]Departament de Química Inorgànica, Facultat de Química, Universitat de Barcelona, Martí i Franquès 1-11, E-08028 Barcelona, Spain

[∥]School of Chemistry and Molecular Biosciences, University of Queensland, Brisbane, Queensland 4072, Australia

Supporting Information

ABSTRACT: The macrobicyclic mixed-donor N_3S_3 cage ligand AMME-N_3S_3sar (1-methyl-8-amino-3,13,16-trithia-6,10,19-triazabicyclo[6.6.6]eicosane) can form complexes with Cu(II) in which it acts as hexadentate (N_3S_3) or tetradentate (N_2S_2) donor. These two complexes are in equilibrium that is strongly influenced by the presence of halide ions (Br^- and Cl^-) and the nature of the solvent (DMSO, MeCN, and H_2O). In the absence of halides the hexadentate coordination mode of the ligand is preferred and the encapsulated complex ("Cu-in^{2+}") is formed. Addition of halide ions in organic solvents (DMSO or MeCN) leads to the tetradentate complex ("Cu-out$^+$") in a polyphasic kinetic process, but no Cu-out$^+$ complex is formed when the reaction is performed in water. Here we applied density functional theory calculations to study the mechanism of this interconversion as well as to understand the changes in the reactivity associated with the presence of water. Calculations were performed at the B3LYP/(SDD,6-31G**) level, in combination with continuum (MeCN) or discrete-continuum (H_2O) solvent models. Our results show that formation of Cu-out$^+$ in organic media is exergonic and involves sequential halide-catalyzed inversion of the configuration of a N-donor of the macrocycle, rapid halide coordination, and inversion of the configuration of a S-donor. In aqueous solution the solvent is found to have an effect on both the thermodynamics and the kinetics of the reaction. Thermodynamically, the process becomes endergonic mainly due to the preferential solvation of halide ions by water, while the kinetics is influenced by formation of a network of H-bonded water molecules that surrounds the complex.

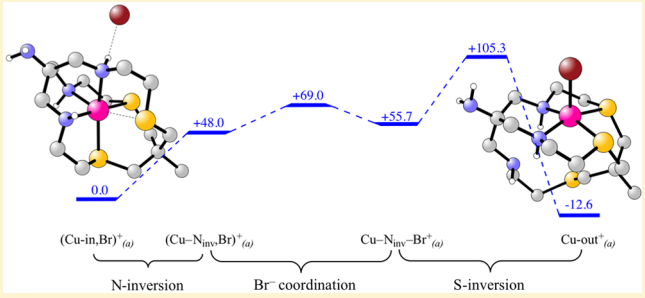

INTRODUCTION

The interaction between metal ions and macrocyclic ligands constitutes a central area in classical coordination chemistry.[1−4] Complexes formed show enhanced thermodynamic and kinetic stabilities with respect to their monodentate counterparts, and the reasons for this are well known. In fact, the stabilizing effect is so pronounced that it even allows observation of unusual metal ion oxidation states and coordination geometries. Nevertheless, in many cases these metal complexes can adopt various molecular structures, the observed form being dependent on the specific media conditions. Thus, chemical (pH gradients, presence of a metal ion, etc.) or physical (light irradiation, flux of electrons, etc.) stimuli can alter the preferred molecular structure and give rise to molecular reorganizations. These processes have been used to generate materials with interesting new properties and a wide range of applications in molecular recognition, enzyme mimicking, molecular devices, and pharmaceutical chemistry.[5,6]

Conversely, ligands from the sarcophagine family (sar, Chart 1) are not prone to such behavior,[7−12] and generally only one molecular structure, which features the metal totally encapsulated by the hexadentate ligand, is found for a range of transition and d-block metal ions. Notably, expanded versions of these cage complexes, i.e., 1,5,5,9,13,13,20,20-octamethyl-3,7,11,15,18,22-hexaazabicyclo[7.7.7]tricosane (Me_8tricosaneN_6), have been found to differ in this behavior and encapsulate transition metal atoms in a variety of geometries where the ligand acts as either hexadentate or pentadentate.[13,14] The chemistry of the first type of these species has shown unique physical properties, such as enhanced thermodynamic stability and extreme resistance to dissociation, which have, for instance, important applications in medicinal chemistry by complexation of ^{64}Cu(II) for diagnostic positron emission tomography (PET) imaging.[15] Indeed, demetalation of hexadentate cage complexes requires harsh reaction conditions such as concentrated acid, extraction of the metal with highly competitive ligands, or redox processes that liberate the metal center.[16] Although these reactions must occur via partially (e.g., tetradentate) coordinated forms of the ligand,

Received: October 7, 2013
Published: December 19, 2013

   dx.doi.org/10.1021/ic402533j | Inorg. Chem. 2014, 53, 512−521

Chart 1

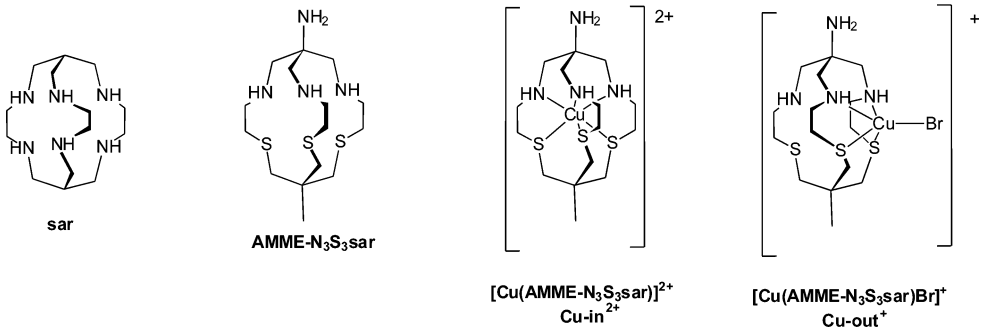

identification of the intermediates is difficult given the conditions required.

We have been involved in the study of formation and isomerization behavior of transition metal complexes of a diversity of centers and macrocyclic N- and S-donor ligands.[17−19] Furthermore, we recently reported that the mixed-donor ligand AMME-N_3S_3sar (1-methyl-8-amino-3,13,16-trithia-6,10,19-triazabicyclo[6.6.6]eicosane, Chart 1) encapsulates Cu(II) in a typical hexadentate fashion, generating $[Cu(AMME\text{-}N_3S_3sar)]^{2+}$ (Cu-in^{2+}, Chart 1).[20,21] However, the competition of a ligand such as Br^- has shown that the macrocycle can also act as a tetradentate-N_2S_2 ligand (eq 1) in the square pyramidal $[Cu(AMME\text{-}N_3S_3sar)Br]^+$ bromido complex (Cu-out$^+$, Chart 1). Cu-out$^+$ has the Cu atom perched on an outer face of the tetradentate-coordinated cage and, noticeably, constitutes a putative intermediate in the demetalation process of Cu-in^{2+}. It is also worth indicating that for these complexes the N and S donors are chirotopic centers, and therefore, the equilibrium in eq 1 involves not only halide coordination but also inversion of one amine and one sulfur donor on the same ligand strap. Nevertheless, the two species have been shown to be in a delicate equilibrium, and while Cu-out$^+$ is observed when aprotic solvents such as MeCN or DMSO are employed, the presence of H_2O shifts the equilibrium to Cu-in^{2+}. The importance of this interconversion has led to the report of a detailed kinetic study, which included temperature- and pressure-dependent data for this multistep process, as well as proposing an active role of the solvent.[20] However, given the fact that there is still important mechanistic information that remains unclear, here we report an extensive DFT study aimed to evaluate the feasibility of the previously proposed mechanisms and analyze other possible pathways. In synergic combination with the available experimental information, DFT results have proven to be very useful, allowing us to fully explain the characteristics of the experimental transformations observed.

$$\underset{\text{Cu-in}^{2+}}{[Cu(AMME\text{-}N_3S_3sar)]^{2+}} + Br^- \rightarrow \underset{\text{Cu-out}^{+}}{[Cu(AMME\text{-}N_3S_3sar)Br]^{+}} \quad (1)$$

RESULTS AND DISCUSSION

Geometries of Cu-out$^+$ and Cu-in^{2+}. The computational study was initiated by optimizing the Cu-in^{2+} and Cu-out$^+$ species starting from their X-ray crystal structures obtained at 293 K. Optimizations were initially performed both in the gas phase and in acetonitrile solution, and the corresponding structures have been labeled with the subscripts *(g)* and *(a)*, respectively (see Computational Details). Key structural data obtained are included in Table 1 and Figure 1. Overall, both gas-phase and solution optimizations are in good agreement with the available crystal structure data, although the typical overestimation of the metal−ligand distance associated to the B3LYP functional is observed (see Tables S1 and S2, Supporting Information).[22]

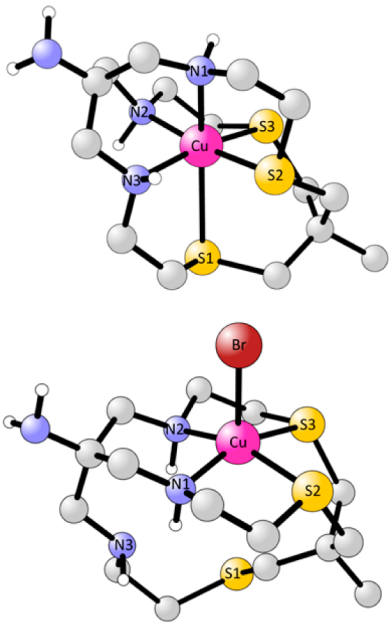

Figure 1. Optimized structures of Cu-in$^{2+}{}_{(a)}$ (up) and Cu-out$^{+}{}_{(a)}$ (down). See Table 1 for structural data. Carbon-bound hydrogen atoms have been omitted for clarity.

The structure of Cu-in^{2+} requires special attention; despite the fact that its X-ray structure collected at 293 K shows three similar Cu−N and Cu−S bonds and a trigonal symmetry, EPR experiments have demonstrated that the real complex has the Cu(II) in a tetragonally elongated (4 + 2) environment typically associated with Jahn−Teller distortions.[23−25] Such "unusual" XRD-determined structures have already been observed for other Cu polyamine complexes, the effect being derived from a very low activation barrier for interconversion between Jahn−Teller enantiomers.[23] Among other techniques, low-temperature EPR spectroscopy provides a simple way of characterizing such effect, as a phase change is observed at low temperatures when a static structure is achieved. In this respect, EPR measurements for Cu-in^{2+} between 100 and 293 K do not show phase changes,[21] thus indicating a very facile process. The same conclusion is reached when the transition state for such

dx.doi.org/10.1021/ic402533j | Inorg. Chem. 2014, 53, 512−521

Table 1. Comparison of Cu−N and Cu−S Distances (Å) between the Experimental XRD Analysis and DFT-Optimized Geometries of Cu-in^{2+} and Cu-out^{+} Complexes[a]

	d(Cu−N1)	d(Cu−N2)	d(Cu−N3)	d(Cu−S1)	d(Cu−S2)	d(Cu−S3)	d(Cu−Br)	average d(Cu−N)	average d(Cu−S)
					Cu-in^{2+}				
X-ray	2.114	2.114	2.114	2.471	2.471	2.471		2.114	2.471
Cu-in$^{2+}{}_{(g)}$	2.328	2.075	2.163	2.781	2.395	2.397		2.189	2.524
Cu-in$^{2+}{}_{(a)}$	2.291	2.062	2.155	2.854	2.392	2.403		2.169	2.550
Cu-in$^{2+}{}_{(w)}$	2.312	2.059	2.119	2.838	2.412	2.401		2.163	2.550
					Cu-out^{+}				
X-ray	2.025	1.998			2.312	2.330	2.555		
Cu-out$^{+}{}_{(g)}$	2.085	2.093			2.453	2.410	2.464		
Cu-out$^{+}{}_{(a)}$	2.081	2.067			2.418	2.411	2.602		
Cu-out$^{+}{}_{(w)}$	2.081	2.044			2.403	2.413	2.638		

[a]Geometries with subscript *(g)* correspond to gas-phase optimizations, while those with subscripts *(a)* and *(w)* have been calculated in acetonitrile and water solution, respectively (see Computational Details).

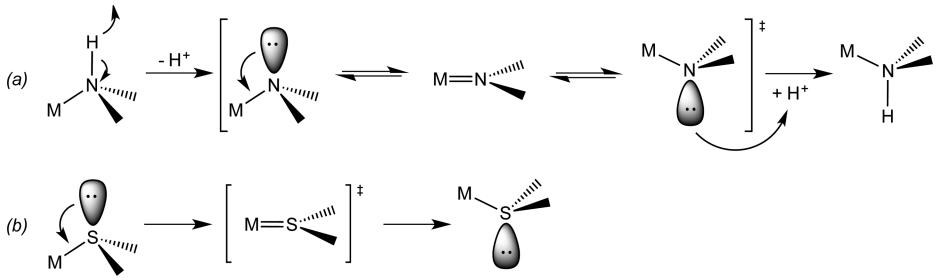

Figure 2. Schematic representation of the N (a) and S inversion (b) of the ligand configuration without undergoing coordinate-bond dissociation.

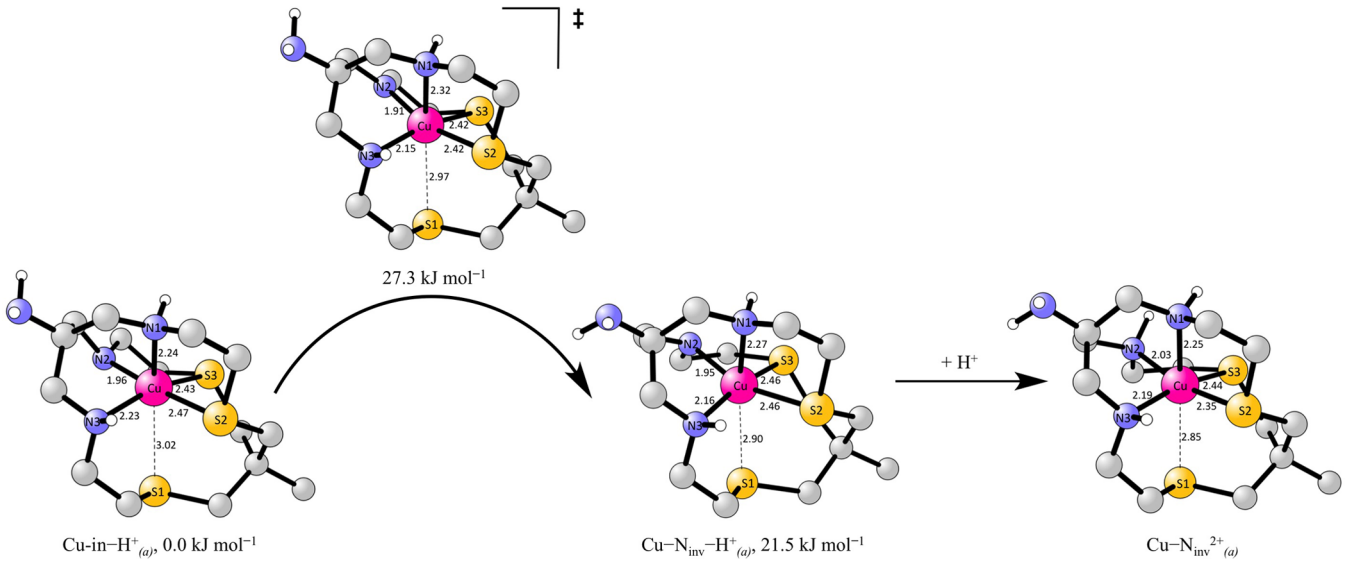

Figure 3. Optimized structures with key distances (Å) of the minima and transition states involved in the N2 inversion of Cu-in$^{2+}{}_{(a)}$. Free energies with respect to Cu-in−H$^{+}{}_{(a)}$ are given in kJ mol^{-1}. Carbon-bound hydrogen atoms have been omitted for clarity.

interconversion is computed; comparison with the ground state geometry leads to an activation barrier of 3.0 kJ mol^{-1} in the gas phase (4.2 kJ mol^{-1} in acetonitrile solution), a value within the range of activation barriers calculated for other Cu(II) polyamine complexes that show the same effect.[26] Thus, while the X-ray-determined structure of Cu-in^{2+} corresponds to an average of the three possible Jahn−Teller enantiomers, each of them featuring four short (equatorial) and two long (axial) bonds, its DFT optimization leads to just one of these isoenergetic enantiomers, the one with longer Cu−S1 and Cu−N1 distances according to the nomenclature in Figure 1 (see Table 1 and average distances for comparisons).

N and S Inversion on Cu-in^{2+}. Although the N and S isomerizations that occur during formation of Cu-out^{+} from Cu-in^{2+} seem to be highly dominated by the presence of Br^{-} anions in acetonitrile or dimethyl sulfoxide solution, the characteristics of the necessary N- and S-inversion processes[20,21] on the Cu-in^{2+} complex have been initially studied in the absence of halides. Kinetico-mechanistic studies on transition metal complexes with polyamine ligands have shown that in aqueous media N inversions can be catalyzed by both acid and base.[27,28] Base-catalyzed isomerization is generally faster and takes place by an internal conjugate base mechanism,[29,30] in which hydroxide ion deprotonates an

dx.doi.org/10.1021/ic402533j | Inorg. Chem. 2014, 53, 512−521

amine (coordinated to a *trivalent* metal ion) and generates an intermediate that undergoes inversion of the nitrogen configuration. For instance, detailed studies on the isomerization kinetics of Cu(II) complexes of both *meso* and *rac* isomers of the tetraamine macrocyclic ligand $Me_6[14]aneN_4$ from a folded to a planar conformation have shown that the processes are catalyzed by base.[30] On the other hand, in water the acid-catalyzed N inversion involves dissociation of the nitrogen donor and rapid proton equilibration of the amino group; ring closure ultimately leads to the N-inverted product. In this sense, it is known that complex $[Cu(sar)]^{2+}$ undergoes a relatively facile detachment of a ligand strap in acid solution, giving a species with a different bound-N configuration.[14,31,32] However, in nonprotic solvents N inversion might be facilitated by abstraction of a proton to form a temporary amide ion in which the nitrogen can invert and be reprotonated (Figure 2a) in a process rather similar to the above-mentioned internal conjugate base mechanism. Since proton abstraction is not a facile process in solvents with poor protophilicity such as MeCN or DMSO and the fact that the metal ion is only divalent thus having little influence on the N–H bond strength, this reaction is expected not to be favored under these conditions.[33,34]

With these facts in mind, the ground state species and transition states involved in inversion of the configuration of the donor N2 of Cu-in^{2+} (Figure 1) have been optimized in acetonitrile solution, and their structures are shown in Figure 3. Deprotonation of N2 generates species Cu-in–$H^+_{(a)}$, which features a shorter Cu–N2 bond (1.96 Å, cf. 2.15 Å), as expected from the representation in Figure 2a, while the remaining Cu–N and Cu–S bonds became longer by ca. 0.1–0.2 Å due to inductive effects. Due to its inherent complexity,[35] we have not calculated the free energy change associated to the ionization processes. Cu-in–$H^+_{(a)}$ can then isomerize through a transition state that has N2 in a planar environment (the N2–C_{adj1}–C_{adj2}–Cu dihedral angle being 1.1°), while the Cu–N and Cu–S distances remain quite similar to those in Cu-in–$H^+_{(a)}$ (see Figure 3). Energetically, this transition state is only 27.3 kJ mol^{-1} higher than Cu-in–$H^+_{(a)}$, indicating that once deprotonation has taken place isomerization occurs readily to produce Cu–N_{inv}–$H^+_{(a)}$. Interestingly, N2 inversion also promotes an important change in the complex structure, which goes from lel_3 to lel_2ob. The *lel* (parallel) and *ob* (oblique) nomenclature refers to the parallel or oblique orientation of the C–C bond connecting the N and S donors of each strap of the macrocycle with respect to the pseudo-C_3 axis of the complex.[36,37] It is known that copper hexamine cage complexes have a general preference for the lel_3 geometry, and the same conclusion seems to apply to this system as, in spite of Cu-in–$H^+_{(a)}$ and Cu–N_{inv}–$H^+_{(a)}$ showing very similar Cu–N and Cu–S distances, the latter is 21.5 kJ mol^{-1} higher in energy. Protonation of Cu–N_{inv}–$H^+_{(a)}$ generates Cu–$N_{inv}{}^{2+}_{(a)}$, which is 30.3 kJ mol^{-1} less stable than Cu-$in^{2+}_{(a)}$, again such difference being associated to the lel_2ob coordination mode of the ligand.

The situation changes significantly when the inversion of the configuration of one of the S donors in Cu-in^{2+} is considered. Given the fact that the sulfur donors have two lone electron pairs (one of which is coordinated to the metal ion), inversion can occur without hydrogen ion abstraction or bond dissociation, as illustrated schematically in Figure 2b.[38] Figure 4 shows the structures of the transition state (TS–Cu–$S_{inv}{}^{2+}_{(a)}$) and final product (Cu–$S_{inv}{}^{2+}_{(a)}$) for inversion of the

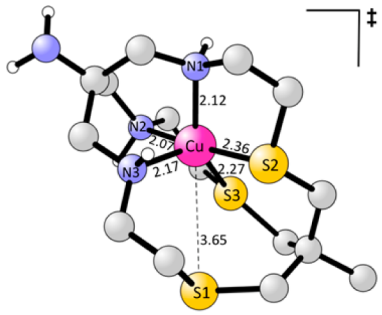

TS–Cu–$S_{inv}{}^{2+}_{(a)}$, +101.1 kJ mol^{-1}

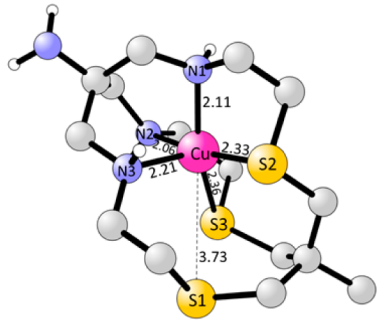

Cu–$S_{inv}{}^{2+}_{(a)}$, +47.1 kJ mol^{-1}

Figure 4. Optimized structures with key distances (Å) of the transition state (TS–Cu–$S_{inv}{}^{2+}_{(a)}$, up) and product (Cu–$S_{inv}{}^{2+}_{(a)}$, down) of the S3 inversion in Cu-$in^{2+}_{(a)}$. Free energies with respect to Cu-$in^{2+}_{(a)}$ are given in kJ mol^{-1}. Carbon-bound hydrogen atoms have been omitted for clarity.

configuration of S3 in complex Cu-$in^{2+}_{(a)}$. TS–Cu–$S_{inv}{}^{2+}_{(a)}$ is 101.0 kJ mol^{-1} less stable than the reactant in free energy terms and shows small changes in the Cu–S2 distance (2.36 Å, cf. 2.39 Å for Cu-$in^{2+}_{(a)}$) as well as the expected planar arrangement of S3 (the S3–C_{adj1}–C_{adj2}–Cu dihedral angle being 5.2°). Interestingly, the corresponding enthalpy of activation is 100.0 kJ mol^{-1}, a value only 1.0 kJ mol^{-1} lower than the free energy barrier that points toward a negligible entropy change. Steric reasons force donor S1 to dissociate from the metal center in the product Cu–$S_{inv}{}^{2+}_{(a)}$. This species is 47.1 kJ mol^{-1} less stable than the reactant and features the macrocyclic ligand in a pentadentate fashion. Its coordination geometry is close to square planar (τ = 0.25),[39,40] with the S2, S3, N1, and inverted N2 donors in the equatorial plane and N3 occupying the axial position.

Thus, these calculations emphasize the stability of Cu-in^{2+} as a definite entity and indicate that inversion of the configuration of the N and S donors of the macrocycle is not a favorable process in the absence of other species in noncoordinating solvents.

Cu-in^{2+}/Br^-/Cu-out^+ Equilibrium in MeCN or DMSO. Kinetic experiments carried out in MeCN and DMSO solution have shown that under an excess of bromide anions complex Cu-in^{2+} is neatly converted to Cu-out^+ in a process that involves two consecutive steps (eq 2). Values obtained for the different rate constants indicate that, for the first step, the process is linearly dependent on the bromide concentration (k in M^{-1} s^{-1}), while the second step shows a value of the rate constants that is bromide concentration independent (k in s^{-1}, see Table 2). As indicated above, the chirality of each coordinated N and S donor[18,41] forces inversion of one

dx.doi.org/10.1021/ic402533j | Inorg. Chem. 2014, 53, 512–521

Table 2. Summary of the Kinetic and Thermal and Pressure Activation Parameters Determined for the System Indicated in Eq 1 (Chart 1) in a Variety of Solvents and with Different Halide Ions[a]

solvent	halide	step	$10^3 \times {}^{298}k$	$\Delta H^{\ddagger}$/kJ mol^{-1}	$\Delta S^{\ddagger}$/J K^{-1} mol^{-1}	$\Delta V^{\ddagger}$/cm^3 mol^{-1}
DMSO	Br^-	first *on*	83 M^{-1} s^{-1}	97 ± 13	60 ± 42	−16 ± 4
		second	0.30 s^{-1}	90 ± 1	−11 ± 5	−3 ± 1
	Cl^-	first *on*	3800 M^{-1} s^{-1}	47 ± 4	−78 ± 13	*b*
		second	29 s^{-1}	38 ± 4	−166 ± 12	*b*
MeCN	Br^-	first *on*	200 M^{-1} s^{-1}	57 ± 3	−69 ± 12	6 ± 1
		second	0.28 s^{-1}	equivalence with the data in DMSO solution	equivalence with the data in DMSO solution	equivalence with the data in DMSO solution
DMSO	none	*c*	1.6 s^{-1}	75 ± 7	−20 ± 24	*b*
MeCN	none	*c*	1.1 s^{-1}	98 ± 7	24 ± 23	∼0

[a]Data from ref 20. [b]Not measured. [c]A single reaction is observed.

amine and one sulfur donor of one of the ligand straps in Cu-in^{2+} (i.e., N1 and S2 in Figure 1). As Br^- coordination to Cu(II) centers is known to be much faster than any of the two experimental kinetic rate constants measured, the two steps have been previously assigned to inversions of the configuration of those donors.[20]

Interestingly, a very clear effect in the near-UV region of the UV−vis spectrum of Cu-in^{2+} is observed during the N- and S-inversion processes. While the spectral changes in this region are almost negligible during the first step of the reaction, where two charge-transfer bands are present, in the second kinetic step one of them disappears. Such bands have been proposed to correspond to S → Cu transitions,[20,21] therefore supporting a mechanism in which N inversion takes place prior S inversion (eq 2). Computation of the theoretical absorption spectra of Cu-in$^{2+}{}_{(a)}$, Cu−$N_{inv}{}^{2+}{}_{(a)}$, and Cu−$S_{inv}{}^{2+}{}_{(a)}$ by means of TD-DFT calculations (see Figure S1, Supporting Information) corroborates that the number of absorption bands in this region of the UV−vis spectrum depends on the number of equivalent S-donor ligands: while the theoretical spectra of Cu-in$^{2+}{}_{(a)}$ and Cu−$N_{inv}{}^{2+}{}_{(a)}$ shows two charge-transfer bands between 300 and 400 nm, the spectrum of Cu−$S_{inv}{}^{2+}{}_{(a)}$ shows only one.

$$\text{Cu-in}^{2+} + \text{Br}^- \rightarrow \text{intermediate} \rightarrow \text{Cu-out}^{+} \qquad (2)$$

The thermal and pressure activation parameters shown in Table 2 have been found to support this reaction mechanism. The calculations described in the previous section indicate that inversion of the configuration of the N donors in Cu-in^{2+} requires an external base able to abstract the proton of the amine. While bromide ions are relatively weak bases in water, this is not so in organic solvents, the pK_a of HBr in MeCN and DMSO being 5.5 and 0.9, respectively.[42,43] The experimental $\Delta H^{\ddagger}$ for the first step of the reaction in MeCN and DMSO (57 and 97 kJ mol^{-1}, respectively, Table 2) agrees with such pK_a difference and effectively supports bromide anions as the proton abstractor agent of the process. A similar conclusion can be inferred when $\Delta H^{\ddagger}$ values for the first step of the reaction with bromide and chloride in DMSO are compared ($\Delta H^{\ddagger}$ is 47 kJ mol^{-1} for Cl^-; pK_a of HCl in DMSO being 1.8).[42] On the other hand, data collected for the second step in Table 2 are also in very good agreement with those calculated for the S inversion in Cu-in^{2+}, i.e., solvent independence and $\Delta S^{\ddagger}$ and $\Delta V^{\ddagger}$ close to zero (as stated above).

In order to prove the viability of the mechanism shown in Scheme 1 we carried out DFT calculations in acetonitrile solution including a bromide ion interacting with the metal complex. Figure 5 (blue) shows the free energy profile associated with this process, and Figure 6 includes the

Scheme 1

$$(\text{Cu-in,Br})^{+}{}_{(a)} \xrightarrow{N\ inversion} (\text{Cu}-N_{inv},\text{Br})^{+}{}_{(a)} \xrightarrow{Br^-\ coordination} \text{Cu}-N_{inv}-\text{Br}^{+}{}_{(a)} \xrightarrow{S\ inversion} \text{Cu-out}^{+}{}_{(a)}$$

corresponding optimized structures. As the N inversion of Cu-in$^{2+}{}_{(a)}$ has already been shown to take place in acetonitrile solution (see Figure 3) via sequential nitrogen deprotonation/inversion/protonation, only the structures of Cu-in$^{2+}{}_{(a)}$ and Cu−$N_{inv}{}^{2+}{}_{(a)}$ ion paired with a bromide anion (i.e., (Cu-in,Br)$^{+}{}_{(a)}$ and (Cu−N_{inv},Br)$^{+}{}_{(a)}$, respectively) have been computed here. Comparison between those indicates that the ion-paired structures are not affected to a large extent by the presence of the halide, and they continue to be *lel*$_3$ and *lel*$_2$*ob*, respectively; furthermore, the main distances and angles remain relatively unchanged. Note that although (Cu−N_{inv},Br)$^{+}{}_{(a)}$ is 48.0 kJ mol^{-1} less stable than (Cu-in,Br)$^{+}{}_{(a)}$ according to the calculations, this difference has to be taken with some caution as the bromide ion has been intentionally placed in the face of the complex from which subsequent bromide ion coordination is favored, but lower energy conformations may exist. Bromide ion coordination from (Cu−N_{inv},Br)$^{+}{}_{(a)}$ takes place via transition state TS−Cu−N_{inv}−$Br^{+}{}_{(a)}$, in which the halide approach (Cu···Br = 3.35 Å) leads to dissociation of the Cu−N3 bond (Cu···N3 = 3.32 Å). The process has a very low activation barrier (21.0 kJ mol^{-1}), thus confirming that once the N inversion has occurred bromide coordination is fast. The product of the bromide ion coordination process Cu−N_{inv}−$Br^{+}{}_{(a)}$ is only 7.7 kJ mol^{-1} less stable than its predecessor (Cu−N_{inv},Br)$^{+}{}_{(a)}$ and features a trigonal bipyramidal structure (τ = 0.07)[39,40] where N1, S2, and Br occupy the equatorial positions while N2 and S3 are axially coordinated. Note that at this point of the reaction the ligand strap that includes the N3 and S1 donors is fully unbound and that S2 inversion leads to the final Cu-out$^+$. The transition state for this final step (TS−Cu−N_{inv}−S_{inv}−$Br^{+}{}_{(a)}$) appears 105.3 kJ mol^{-1} above the reactant (Cu-in,Br)$^{+}{}_{(a)}$ and again has a structure very similar to that calculated for S inversion of Cu-in$^{2+}{}_{(a)}$; the Cu−S2 distance is 2.34 Å (cf. 2.27 Å), and the dihedral angle S2−C_{adj1}−C_{adj2}−Cu is 3.8° (cf. 5.2°). These results seem to indicate that the S-inversion process on these species is not affected in a great extent by the specific characteristics of the macrocycle, and indeed, formation of both Cu−S_{inv}−$Br^{+}{}_{(a)}$ and Cu−$S_{inv}{}^{2+}{}_{(a)}$ species show similar activation barriers (105.3 and 101.0 kJ mol^{-1}, respectively). Finally, the resulting product Cu-out$^{+}{}_{(a)}$ is only 12.6 kJ mol^{-1} less stable than (Cu-in,Br)$^{+}{}_{(a)}$, which accounts for the observed reversibility of the process in eq 1.

Cu-in/Br^-/Cu-out$^+$ Equilibrium in H_2O. While the reaction indicated in eq 1 is largely displaced toward Cu-out$^+$

dx.doi.org/10.1021/ic402533j | Inorg. Chem. 2014, 53, 512−521

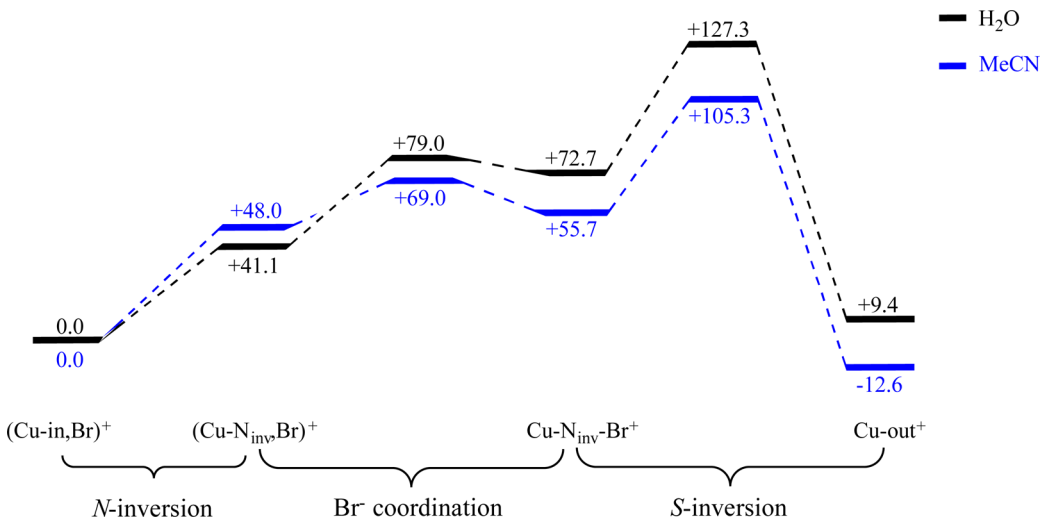

Figure 5. Free energy profiles (kJ mol^{-1}) for formation of Cu-out^{+} from Cu-in^{2+} interacting with a bromide anion according to Scheme 1. Profile in blue corresponds to optimizations in acetonitrile solution, while profile in black corresponds to optimizations in aqueous solutions and includes two explicit H_2O molecules (see Computational Details). Only reactant and product of the N-inversion step have been computed.

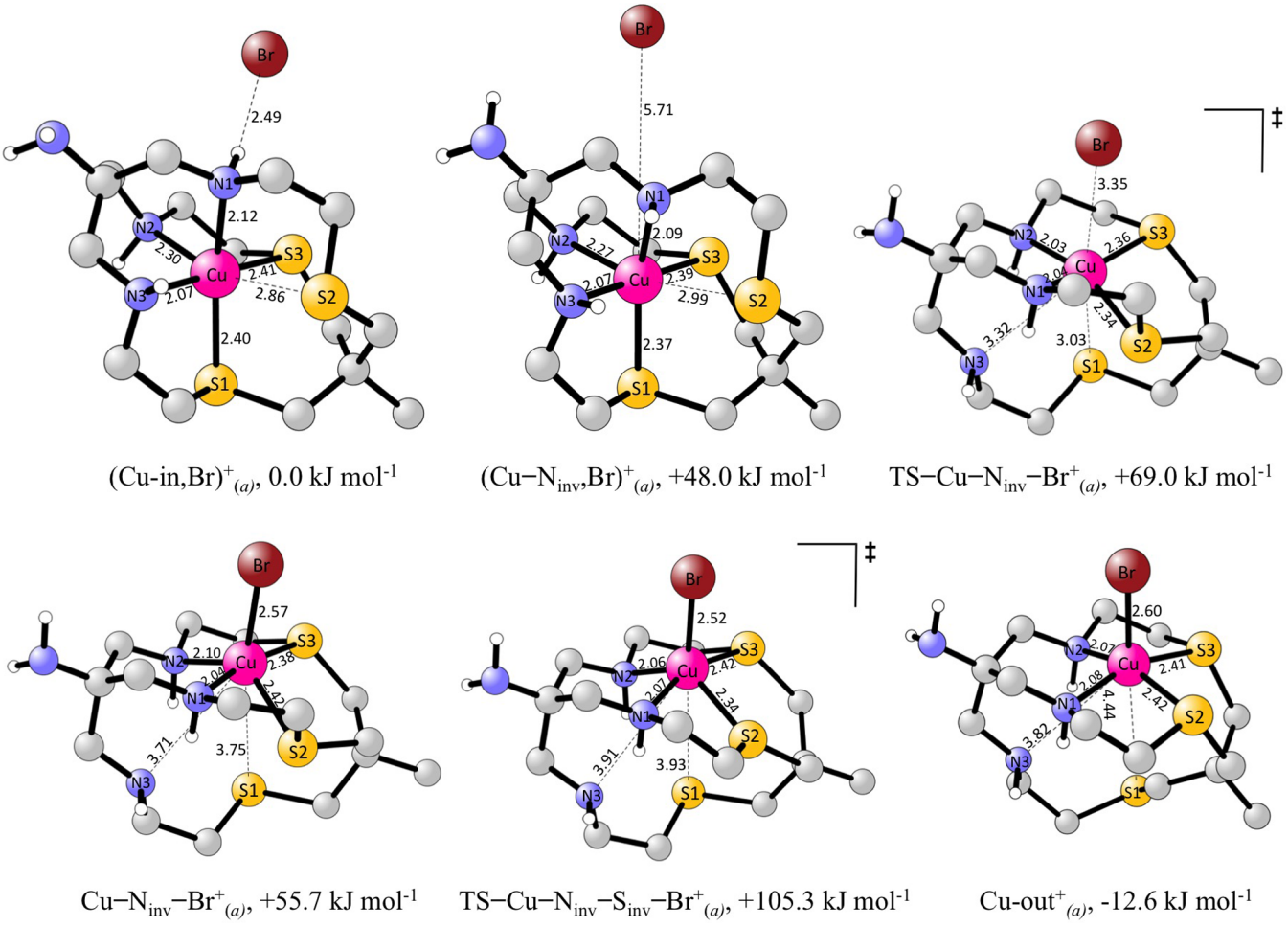

Figure 6. Optimized structures with key distances (Å) of the energetic profile in blue (MeCN solution) of Figure 5. Free energies with respect to $(Cu\text{-}in,Br)^{+}_{(a)}$ are given in kJ mol^{-1}. Carbon-bound hydrogen atoms have been omitted for clarity.

in conditions of an excess of bromide ions using MeCN or DMSO as solvent,[21] when the same reaction is performed in aqueous media, EPR experiments indicate that no Cu-out^{+} is formed.[20] Furthermore, kinetic experiments at different pHs have shown the appearance of small absorbance changes that fit to a single kinetic step only when a large excess of bromide ions is employed. These changes do not show the coalescence of the two charge-transfer bands in the near-UV region, and therefore,

dx.doi.org/10.1021/ic402533j | Inorg. Chem. 2014, 53, 512−521

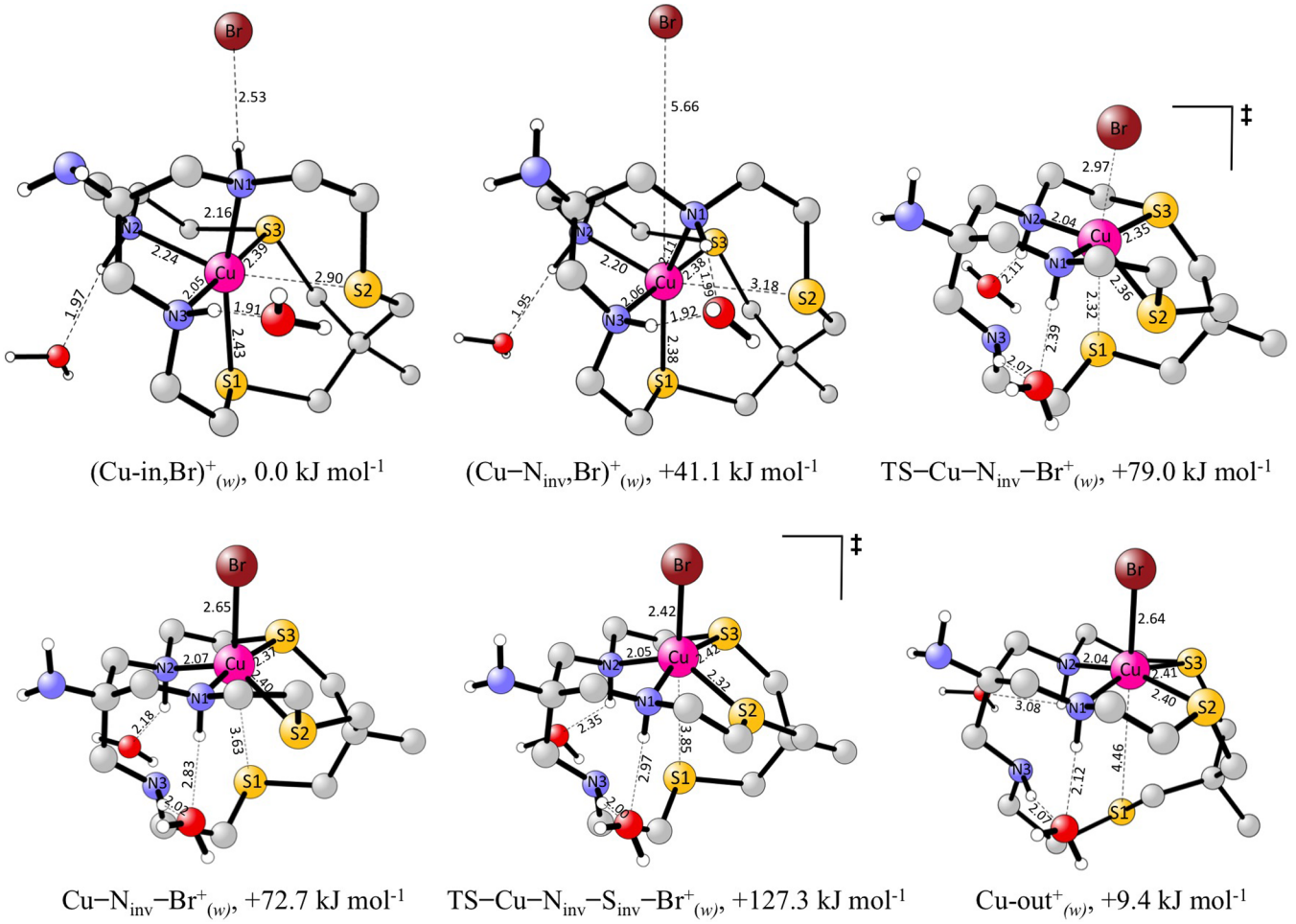

Figure 7. Optimized structures with key distances (Å) of the energetic profile in black (H_2O solution) of Figure 5. Free energies with respect to $(Cu\text{-}in,Br)^+_{(w)}$ are given in kJ mol^{-1}. Carbon-bound hydrogen atoms have been omitted for clarity.

it was proposed that only the first step of the reaction takes place under these conditions.

Obviously, changes in solvent properties can lead to thermodynamic and/or kinetic effects on the reaction.[44] Thermodynamically, it is evident that solvation free energies of the species involved in the equilibrium change on going from MeCN or DMSO to H_2O. While this value is not expected to be much altered for $Cu\text{-}in^{2+}$ and $Cu\text{-}out^+$ species, halide ions have a definite preference for protic solvents. Specifically, the solvation free energy associated to the change from MeCN to H_2O for bromide ions has been determined as −31.4 kJ mol^{-1},[45] and as formation of $Cu\text{-}out^+$ implies a formal bromide ion removal from solution, the higher bromide stability in H_2O has a negative impact on the stability of $Cu\text{-}out^+$ with respect to the reactants. This value seems to be enough to displace eq 1 fully toward the reactants, thus explaining the absence of $Cu\text{-}out^+$ in aqueous media. Furthermore, the presence of H_2O is also expected to modify the structure and relative stability of the intermediate species, mainly due to H-bonding interactions.[46] In an effort to account for these explicit H_2O interactions we recalculated the energy profile associated with the reaction, including two hydrogen-bonded H_2O molecules to two of the NH groups of the ligand and using the PCM parameters for water (see Computational Details). Protonation of the apical NH_2 group has not been considered; in complexes of the same family these groups show a very low basicity,[7] thus making the process only relevant under acidic conditions. A comparison between the energy profiles of the reaction in acetonitrile and water is shown in Figure 5. In good agreement with the experiments, $Cu\text{-}out^+_{(w)}$ becomes slightly less stable than $(Cu\text{-}in,Br)^+_{(w)}$, by 9.4 kJ mol^{-1};[47] Figure 7 collects the structures of the species involved in the energy profile. The structure of the $(Cu\text{-}in,Br)^+_{(w)}$ ion pair shows the implication of the three secondary amine groups in H-bonding interactions; N1 to the bromide ion (Br···HN1 = 2.53 Å) and N2 and N3 to the two explicitly included H_2O molecules (O···HN2 = 1.97 Å and O···HN3 = 1.91 Å). Cu–N and Cu–S distances for this species are indicated in Table 1 and do not show significant differences with respect to the alternative MeCN optimizations, thus indicating that at this stage of the process the presence of H_2O does not have a major effect on the complex structure. Similar conclusions are obtained when the product of the N1 inversion [$(Cu–N_{inv},Br)^+_{(w)}$, +41.1 kJ mol^{-1}; Figure 7] is computed with this methodology. Interestingly, this species has both N1 and N3 donors H bonded to the same H_2O molecule (O···HN1 = 1.99 Å and O···HN3 = 1.92 Å), while N2 continues interacting with the remaining H_2O molecule (O···HN2 = 1.95 Å). Summarizing, as indicated above, the decrease of Lewis basicity of bromide ions on going from aprotic solvents to water retards the actuation of an N inversion catalyzed by halide ions in water. Effectively, the kinetic experiments carried out in excess of chloride or bromide ions in

dx.doi.org/10.1021/ic402533j | Inorg. Chem. 2014, 53, 512−521

water at different pHs show no significant differences between the second-order rate constants for Cl^- and Br^- ions; instead, the reaction accelerates under basic conditions, as expected for the general base-catalyzed N inversion of polyamine ligands in aqueous media.

The main difference between the two energy profiles in Figure 5 relates to the bromide ion coordination to $(Cu-N_{inv},Br)^+_{(a)}$ and $(Cu-N_{inv},Br)^+_{(w)}$. In acetonitrile solution this step occurs readily, producing $Cu-N_{inv}-Br^+_{(a)}$, with a square pyramidal structure and free energy very similar to the starting ion pair; in aqueous solution the activation barrier for the bromide almost doubles, and the corresponding product also becomes relatively less stable (+72.7 vs +55.7 kJ mol^{-1}). Analysis of the structures involved (Figure 7) indicates that the H-bonding interactions of the N donors with the external H_2O molecules play a major role in these differences. Formation of the square pyramidal species $Cu-N_{inv}-Br^+_{(w)}$ forces the metal center to adopt a perched position on the macrocycle, which in turn induces a conformational change of the macrocycle, as the lone pairs of the donors have to keep their orientation to the metal center. Even more noticeable, the reorientation forced onto the secondary amine donors N1 and N2 completely hampers their participation in H-bonding interactions with external H_2O molecules, that is, while $(Cu-N_{inv},Br)^+_{(w)}$ has three H-bonding interactions with NH···O distances in the 1.90−2.00 Å range, none of them are within this range in both $TS-Cu-N_{inv}-Br^+_{(w)}$ and the final $Cu-N_{inv}-Br^+_{(w)}$. As a whole, despite the limitations of the computational model, the results agree with the "enhanced" high stability of the Cu-in^{2+} species in aqueous solutions, including the concept of a shell of H_2O molecules producing further stabilization.

Reactivity of Cu-in^{2+} in the Absence of Halide Ions. One of the most surprising observations of the kinetic experiments carried out on the Cu-in^{2+}/Br^-/Cu-out^+ equilibration relates to the fact that some reactivity of the Cu-in^{2+} complex is observed in the absence of halide anions (see last two entries in Table 2). When a concentrated solution of Cu-in^{2+} in MeCN or DMSO is diluted in the same solvent, small spectral changes, characteristic of a displacement to the right of eq 1, are found that can be fit to a single kinetic step. Interestingly, when dilution is carried out with water, those changes (featuring kinetic traces that can also be fitted to a single step) have opposite characteristics (i.e., they show a displacement to the left of eq 1) and are base-catalyzed.[20] Monitoring these dilutions by EPR spectroscopy does not show formation of any new species, which is a clear indication that the reaction only takes place to a small extent.

In spite of this fact, our interest in the nature of this process led us to analyze a series of hypotheses that could explain these observations. These were (i) coordination of solvent molecules, (ii) a change in the relative stability of the lel_3 conformation of Cu-in^{2+} with respect to lel_2ob, $lelob_2$, and ob_3, and (iii) change in the relative stability of Cu-in^{2+} with respect to $Cu-N_{inv}{}^{2+}$. The first possibility seems unlikely since the EPR spectrum of Cu-in^{2+} does not change after dilution. This has been confirmed by performing DFT optimizations in which explicit MeCN and water molecules were coordinated to the metal center. In both cases decoordination of the solvent molecule took place without any activation barrier, regenerating the Cu-in^{2+} complex H bonded to the solvent molecule. Regarding the stability of the lel_3 conformation of Cu-in^{2+}, literature data show that this is the most stable conformation regardless of the solvent employed,[37] and other conformers have only been observed when the macrocycle suffers from severe steric restrictions. The third hypothesis, a change in the relative stability of Cu-in^{2+} with respect to $Cu-N_{inv}{}^{2+}$ due to the change in the solvent properties, seems the most plausible explanation. As indicated above, the small spectral changes associated with the reaction and the lack of changes in the EPR spectra indicate that such differences in stability are not expected to be large. In agreement with this assumption and in spite of the different sources of error associated to the calculations, computation of Cu-in^{2+} and $Cu-N_{inv}{}^{2+}$ in acetonitrile and water shows a relative stability difference of only 6.0 kJ mol^{-1} when changing MeCN for water, i.e., while $Cu-N_{inv}{}^{2+}{}_{(a)}$ is 30.3 kJ mol^{-1} less stable than Cu-$in^{2+}{}_{(a)}$, this difference decreases to 24.3 kJ mol^{-1} when comparing $Cu-N_{inv}{}^{2+}{}_{(w)}$ with Cu-$in^{2+}{}_{(w)}$. Other indications of this equilibrium are given by the kinetic experiments in terms of the process being base catalyzed, typical of the inversion of amines in water[27,28] and the lack of coalescence of the two charge-transfer bands in near-UV region of the recorded UV−vis spectra, which agrees with the TD-DFT-calculated spectra of these two species (see Figure S1, Supporting Information).

CONCLUSIONS

By the use of DFT calculations, we probed the reported mechanism of interconversion between hexadentate (N_3S_3, Cu-in^{2+}) and tetradentate (N_2S_2, Cu-out^+) Cu(II) complexes of AMME-N_3S_3sar as well as the effect of solvent on their relative stability. Formation of Cu-out^+ from Cu-in^{2+} in the presence of bromide ions is exergonic in acetonitrile and dimethyl sulfoxide media and involves (i) bromide-catalyzed inversion of the configuration of one of the N donors, (ii) rapid bromide ion coordination, and (iii) inversion of the configuration of one of the coordinated S donors. Calculations employing a discrete-continuum solvent model show that in water the reaction becomes endergonic, mainly due to preferential solvation of bromide ions by water. Comparison of the energetic profiles and their associated structures in MeCN and H_2O indicates that, after N inversion, the process is hampered in water due to the presence of hydrogen-bonding interactions between the complex and the water molecules of the medium. The structure and stability of Cu-in^{2+} in the absence of halide ions in MeCN and H_2O has also been analyzed, and a solvent-dependent relative free energy with respect to the N-inverted intermediate has been postulated to explain the spectral changes that appear after dilution of Cu-in^{2+} in different solvents.

EXPERIMENTAL SECTION

Computational Details. All calculations shown in this manuscript were performed using hybrid DFT with the B3LYP exchange-correlation functional[48,49] and the Gaussian 09 Package (Revision A.02).[50] Spin-unrestricted calculations were performed for the paramagnetic species. Cu, S, and Br centers were described with the Stuttgart RECPs and associated basis sets,[51] with added d-orbital polarization on S (ζ = 0.503) and Br (ζ = 0.428).[52] 6-31G** basis sets were used for all other atoms.[53,54] Note that in spite of the slight overestimation of the metal−ligand bond distances calculated at this level of theory and typically associated to use of the B3LYP functional,[22] test calculations with other functionals (see Table S1, Supporting Information) and basis sets on the N and S atoms (see Table S2, Supporting Information) were found not to improve significantly the quality of the results.

Reactivity in organic media (i.e., acetonitrile or DMSO) was modeled by performing the optimizations with the effects of acetonitrile solvent included self-consistently through the polarized

dx.doi.org/10.1021/ic402533j | Inorg. Chem. 2014, 53, 512−521

continuum model (PCM) procedure (standard options, ε = 35.688),[55] and the corresponding calculated structures are labeled with the subscript *(a)*. Gas-phase optimizations were also conducted for comparative purposes, and the corresponding calculated structures are labeled with the subscript *(g)*. Due to the importance of H-bonding interactions in water, reactivity in this media was modeled by including a combination of *nonspecific* and *specific* solvent interactions during the optimizations.[46] For this purpose, two explicit water molecules were included in the computational system and the bulk solvent effect was accounted by the polarized continuum model (PCM, standard options, ε = 78.3553).[55] Structures derived from this methodology are labeled with the subscript *(w)*.

All stationary points were optimized without symmetry constraints and characterized via analytical frequency calculations as either minima (all positive eigenvalues) or transition states (one negative eigenvalue), and IRC calculations were performed on selected transition states to confirm their connection to the minima. Unless otherwise stated, thermodynamic data are reported throughout as free energies at 298.15 K and 1 atm derived from optimization in solution (i.e., acetonitrile or water). In addition, although for this particular system inclusion of dispersion energy corrections only lead to relatively small changes on the computed values, in all cases single-point dispersion corrections using Grimme's D3(BJ) approach[56] were calculated and added to the free energies in solution.

Electronic absorption spectra of the previously optimized species Cu-in$^{2+}{}_{(a)}$, Cu−N$_{inv}{}^{2+}{}_{(a)}$, and Cu−S$_{inv}{}^{2+}{}_{(a)}$ were calculated by the time-dependent DFT (TD-DFT) approach[57,58] associated with the polarized continuum model (PCM, acetonitrile as solvent).[55] The energy and oscillator strength of the lowest 40 singlet excitations were calculated for each species. GaussSum 2.2 was employed to draw the absorption spectra.[59] The equation employed by the program to calculate the theoretical spectrum, and the extinction coefficients are based on Gaussian convolution and reported in the open source code of the program (available at http://gausssum.sourceforge.net/). The full width at half-maximum value used for the simulated spectrum was 2000 cm^{-1}.

■ ASSOCIATED CONTENT

Supporting Information

Cartesian coordinates of all computed structures and associated energies as well as functional and basis set testing on Cu-in$^{2+}{}_{(g)}$ and Cu-out$^{+}{}_{(g)}$; plots of the TD-DFT-calculated spectra of Cu-in$^{2+}{}_{(a)}$, Cu−N$_{inv}{}^{2+}{}_{(a)}$, and Cu−S$_{inv}{}^{2+}{}_{(a)}$. This material is available free of charge via the Internet at http://pubs.acs.org.

■ AUTHOR INFORMATION

Corresponding Author

*E-mail: andres.algarra@uca.es.

Present Address

‡Department of Organic Chemistry, Arrhenius Laboratory, Stockholm University, SE-10691 Stockholm, Sweden.

Notes

The authors declare no competing financial interest.

■ ACKNOWLEDGMENTS

Financial support from the Spanish Ministerio de Ciencia e Innovación (CTQ2012-37821-C02-01 and CTQ2011-23862-C2) is gratefully acknowledged.

■ REFERENCES

(1) Lindoy, L. F.; Park, K.-M.; Lee, S. S. *Chem. Soc. Rev.* **2013**, *42*, 1713−1727.

(2) Lehn, J.-M. *Supramolecular Chemistry*; Wiley-VCH: Weinheim, 1995.

(3) Lindoy, L. F.; Dietrich, B.; Viout, P.; Lehn, J.-M. In *The Chemistry of Macrocyclic Ligand Complexes*; VCH and Cambridge University Press: Cambridge, 1989.

(4) Fabbrizzi, L. In *Beauty in Chemistry*; Fabbrizzi, L., Ed.; Springer: *New York*, 2012; Vol. *323*.

(5) *Intelligent Materials*; The Royal Society of Chemistry: Cambridge, 2008.

(6) Kinbara, K.; Aida, T. *Chem. Rev.* **2005**, *105*, 1377−1400.

(7) Bernhardt, P. V.; Bramley, R.; Engelhardt, L. M.; Harrowfield, J. M.; Hockless, D. C. R.; Korybut-Daszkiewicz, B. R.; Krausz, E. R.; Morgan, T.; Sargeson, A. M. *Inorg. Chem.* **1995**, *34*, 3589−3599.

(8) Walker, G. W.; Geue, R. J.; Sargeson, A. M.; Behm, C. A. *Dalton Trans.* **2003**, 2992−3001.

(9) Di Bartolo, N. M.; Sargeson, A. M.; Donlevy, T. M.; Smith, S. V. *J. Chem. Soc., Dalton Trans.* **2001**, 2303−2309.

(10) Angus, P. M.; Elliott, A. J.; Sargeson, A. M.; Willis, A. C. *J. Chem. Soc., Dalton Trans.* **2000**, 2933−2938.

(11) Moghaddas, S.; Hendry, P.; Geue, R. J.; Qin, C.; Bygott, A. M. T.; Sargeson, A. M.; Dixon, N. E. *J. Chem. Soc., Dalton Trans.* **2000**, 2085−2089.

(12) Puchta, R.; Meier, R.; van Eldik, R. *Aust. J. Chem.* **2007**, *60*, 889−897.

(13) Qin, C.-J.; James, L.; Chartres, J. D.; Alcock, L. J.; Davis, K. J.; Willis, A. C.; Sargeson, A. M.; Bernhardt, P. V.; Ralph, S. F. *Inorg. Chem.* **2011**, *50*, 9131−9140.

(14) Engelhardt, L.; Grondahl, L.; Harrowfield, J.; Ralph, S.; Sargeson, A.; Skelton, B.; Sobolev, A.; White, A. *J. Inclusion Phenom. Macrocyclic Chem.* **2011**, *71*, 353−362.

(15) Ma, M. T.; Cooper, M. S.; Paul, R. L.; Shaw, K. P.; Karas, J. A.; Scanlon, D.; White, J. M.; Blower, P. J.; Donnelly, P. S. *Inorg. Chem.* **2011**, *50*, 6701−6710.

(16) Grondahl, L.; Hammershoi, A.; Sargeson, A. M.; Thöm, V. J. *Inorg. Chem.* **1997**, *36*, 5396−5403.

(17) Martínez-Alanis, P. R.; Sánchez Eguía, B. N.; Ugalde-Saldívar, V. M.; Regla, I.; Demare, P.; Aullón, G.; Castillo, I. *Chem.—Eur. J.* **2013**, 6067−6079.

(18) Aullón, G.; Bernhardt, P. V.; Bozoglián, F.; Font-Bardía, M.; Macpherson, B. P.; Martínez, M.; Rodríguez, C.; Solans, X. *Inorg. Chem.* **2006**, *45*, 8551−8562.

(19) Bernhardt, P. V.; Martínez, M.; Rodríguez, C.; Vazquez, M. *Inorg. Chem.* **2010**, *50*, 1429−1440.

(20) Bernhardt, P. V.; Font, H.; Gallego, C.; Martínez, M.; Rodríguez, C. *Inorg. Chem.* **2012**, *51*, 12372−12379.

(21) Bell, C. A.; Bernhardt, P. V.; Gahan, L. R.; Martínez, M.; Monteiro, M. J.; Rodríguez, C.; Sharrad, C. A. *Chem.—Eur. J.* **2010**, *16*, 3166−3175.

(22) Koch, W.; Holthausen, M. C. *A chemist's guide to density functional theory*; Wiley-VCH: New York, 2000.

(23) Halcrow, M. A. *Chem. Soc. Rev.* **2013**, *42*, 1784−1795.

(24) Kundu, T. K.; Manoharan, P. T. *Chem. Phys. Lett.* **1995**, *241*, 627−634.

(25) Donlevy, T. M.; Hambley, T. W.; Hanson, G. R.; McMahon, K. L.; Stranger, R.; Gahan, L. R. *Inorg. Chem.* **1994**, *33*, 5131−5137.

(26) Mack, K.; Wünsche von Leupoldt, A.; Förster, C.; Ezhevskaya, M.; Hinderberger, D.; Klinkhammer, K. W.; Heinze, K. *Inorg. Chem.* **2012**, *51*, 7851−7858.

(27) Tobe, M. L. Academic Press: London, 1983; pp 1−94.

(28) Tobe, M. L.; Burgess, J. *Inorganic Reactions Mechanisms*: Longman: Harlow, U.K., 1999.

(29) Curchod, B. F. E.; Rotzinger, F. P. *Inorg. Chem.* **2011**, *50*, 8728−8740.

(30) Lee, C.-S.; Wang, G.-T.; Chung, C.-S. *J. Chem. Soc., Dalton Trans.* **1984**, 109−114.

(31) Sargeson, A. M. *Pure Appl. Chem.* **1984**, *56*, 1603−1619.

(32) Sargeson, A. M. *Pure Appl. Chem.* **1986**, *58*, 1511−1522.

(33) Kulatilleke, C. P.; Goldie, S. N.; Heeg, M. J.; Ochrymowycz, L. A.; Rorabacher, D. B. *Inorg. Chem.* **2000**, *39*, 1444−1453.

(34) Sanzenbacher, R.; Elias, H. *Inorg. Chim. Acta* **1996**, *246*, 267−274.

(35) Alongi, K. S.; Shields, G. C. In *Annual Reports in Computational Chemistry*; Ralph, A. W.; Elsevier: New York, 2010; Vol. *6*, pp 113−138.
(36) Comba, P. *Coord. Chem. Rev.* **1999**, *182*, 343−371.
(37) Comba, P. *Inorg. Chem.* **1989**, *28*, 426−431.
(38) Aronne, L.; Yu, Q.; Ochrymowycz, L. A.; Rorabacher, D. B. *Inorg. Chem.* **1995**, *34*, 1844−1851.
(39) Parameter σ is defined by the equation $\tau = (\alpha - \beta)/60$, where α and β are the two largest L−M−L bond angles ($\alpha \geq \beta$) of a pentacoordinate complex. This parameter was introduced by Addison et al. (see ref 40) to quantify the structural distortions between the two ideal structures of a pentacoordinate complex, i.e., the trigonal bipyramid (*tbp*) and square pyramid (*sp*). Complexes featuring an ideal *tbp* geometry have $\tau = 1$, those with ideal *sp* geometry have $\tau = 0$, and complexes with intermediate geometries show values between 0 and 1.
(40) Addison, A. W.; Rao, T. N.; Reedijk, J.; van Rijn, J.; Verschoor, G. C. *J. Chem. Soc., Dalton Trans.* **1984**, 1349−1356.
(41) Adams, H.; Amado, A. M.; Félix, V.; Mann, B. E.; Antelo-Martinez, J.; Newell, M.; Ribeiro-Claro, P. J. A.; Spey, S. E.; Thomas, J. A. *Chem.—Eur. J.* **2005**, *11*, 2031−2046.
(42) Bordwell, F. G. *Acc. Chem. Res.* **1988**, *21*, 456−463.
(43) Kütt, A.; Rodima, T.; Saame, J.; Raamat, E.; Mäemets, V.; Kaljurand, I.; Koppel, I. A.; Garlyauskayte, R. Y.; Yagupolskii, Y. L.; Yagupolskii, L. M.; Bernhardt, E.; Willner, H.; Leito, I. *J. Org. Chem.* **2010**, *76*, 391−395.
(44) Marcus, Y. *The properties of solvents*; Wiley: New York, 1998.
(45) Böes, E. S.; Livotto, P. R.; Stassen, H. *Chem. Phys.* **2006**, *331*, 142−158.
(46) Ren, P.; Chun, J.; Thomas, D. G.; Schnieders, M. J.; Marucho, M.; Zhang, J.; Baker, N. A. *Q. Rev. Biophys.* **2012**, *45*, 427−491.
(47) Note that the ion pair $(\text{Cu-in,Br})^{+}_{(w)}$ is unlikely to be formed in water solution due to its dielectric constant; however, we considered it as zero in free energy for comparative purposes.
(48) Becke, A. D. *J. Chem. Phys.* **1993**, *98*, 5648−5652.
(49) Lee, C. T.; Yang, W. T.; Parr, R. G. *Phys. Rev. B* **1988**, *37*, 785−789.
(50) Frisch, M. J.; Trucks, G. W.; Schlegel, H. B.; Scuseria, G. E.; Robb, M. A.; Cheeseman, J. R.; Scalmani, G.; Barone, V.; Mennucci, B.; Petersson, G. A.; Nakatsuji, H.; Caricato, M.; Li, X.; Hratchian, H. P.; Izmaylov, A. F.; Bloino, J.; Zheng, G.; Sonnenberg, J. L.; Hada, M.; Ehara, M.; Toyota, K.; Fukuda, R.; Hasegawa, J.; Ishida, M.; Nakajima, T.; Honda, Y.; Kitao, O.; Nakai, H.; Vreven, T.; Montgomery, Jr., J. A.; Peralta, J. E.; Ogliaro, F.; Bearpark, M.; Heyd, J. J.; Brothers, E.; Kudin; K. N.; Staroverov, V. N. K. R.; Normand, J.; Raghavachari, K.; Rendell, A.; Burant, J. C.; Iyengar, S. S.; Tomasi, J.; Cossi, M.; Rega, N.; Millam, N. J.; Klene, M.; Knox, J. E.; Cross, J. B.; Bakken, V.; Adamo, C.; Jaramillo, J.; Gomperts, R.; Stratmann, R. E.; Yazyev, O.; Austin, A. J.; Cammi, R.; Pomelli, C.; Ochterski, J. W.; Martin, R. L.; Morokuma, K.; Zakrzewski, V. G.; Voth, G. A.; Salvador, P.; Dannenberg, J. J.; Dapprich, S.; Daniels, A. D.; Farkas, O.; Foresman, J. B.; Ortiz, J. V.; Cioslowski, J.; Fox, D. J. *Gaussian 09*, Revision A.02; Gaussian: Wallingford, CT, 2009.
(51) Andrae, D.; Häu*β*ermann, U.; Dolg, M.; Stoll, H.; Preu*β*, H. *Theor. Chim. Acta* **1990**, *77*, 123−141.
(52) Hollwarth, A.; Bohme, M.; Dapprich, S.; Ehlers, A. W.; Gobbi, A.; Jonas, V.; Kohler, K. F.; Stegmann, R.; Veldkamp, A.; Frenking, G. *Chem. Phys. Lett.* **1993**, *208*, 237−240.
(53) Harihanan, P. C.; Pople, J. A. *Theor. Chim. Acta* **1973**, *28*, 213−222.
(54) Hehre, W. J.; Ditchfield, R.; Pople, J. A. *J. Chem. Phys.* **1972**, *56*, 2257−2261.
(55) Tomasi, J.; Mennucci, B.; Cammi, R. *Chem. Rev.* **2005**, *105*, 2999−3093.
(56) Grimme, S.; Antony, J.; Ehrlich, S.; Krieg, H. *J. Chem. Phys.* **2010**, *132*, 154104−154119.
(57) Furche, F.; Ahlrichs, R. *J. Chem. Phys.* **2002**, *117*, 7433−7447.
(58) Casida, M. E.; Jamorski, C.; Casida, K. C.; Salahub, D. R. *J. Chem. Phys.* **1998**, *108*, 4439−4449.
(59) O'Boyle, N. M.; Tenderholt, A. L.; Langner, K. M. *J. Comput. Chem.* **2008**, *29*, 839−845.